Original Research Article

JABFM Journal of Applied Biomaterials & Functional Materials

Nanostructured akermanite glass-ceramic coating on Ti6Al4V for orthopedic applications

Journal of Applied Biomaterials & Functional Materials
1–8

DOI: 10.1177/2280800018793819
journals.sagepub.com/home/jbf
SAGE

Kazem Marzban[1], Sayed Mahmood Rabiee[2], Ebrahim Zabihi[3] and Sara Bagherifard[4]

Abstract

Glass ceramics are widely used to enhance the functionality of inert metallic materials typically used for hard-tissue engineering. Biofunctionality of glass ceramics can in turn be significantly boosted with the addition of trace element dopants. Herein, we synthesized a nanostructured glass ceramic and used magnesium (Mg), which is known to promote osteoblast adhesion and proliferation, for further functionalization. The nanostructured akermanite glass ceramic ($Ca_2MgSi_2O_7$) was used to coat Ti6Al4V substrates by the sol-gel method. Scanning and transmission electron microscopy as well as X-ray diffraction were used to assess the structural morphology and phase composition of the coating, respectively. The micrographs showed a uniform and crack-free coating structure. Atomic force microscopy observation revealed a disordered surface roughness for coated samples. In vitro cytocompatibility tests revealed that Saos-2 cells cultured on bare samples adopted a rounded morphology, whereas cells cultured on the coated samples represented a more spread out configuration and also increased proliferation. The characterizing tests confirmed the efficiency of the synthesis method and the in vitro biocompatibility of the synthesized coating, indicating its suitability to be used for bone implants.

Keywords

Bioceramics, glass ceramic, akermanite, nanostructured coating, sol-gel preparation, implant

Date received: 8 January 2018; revised: 3 July 2018; accepted: 5 July 2018

Introduction

Titanium and its alloys are considered the gold standard for hard-tissue implant technology thanks to their biocompatibility and stable mechanical properties.[1–3] Host tissue response to inert titanium, however, is not always desirable and can often be prone to fibrous tissue encapsulation.[4] Surface treatments introducing bioceramic coatings are commonly used to functionalize the surface of metallic implants to increase their biocompatibility,[5] corrosion resistance,[6] or fixation characteristics.[4]

The most common bioceramic coatings used for orthopedic implants are calcium phosphate (CaP)[7–9] and Si-based glass ceramics.[10–13] Hydroxyapatite (HA)-coated Ti6Al4V, for example, has been accepted as 1 of the most suitable alternative materials for damaged bone tissue.[6] Previous studies have confirmed the bioactivity of Si-based glass ceramics and their positive role in formation of an HA layer on an implant surface after soaking in simulated body fluid (SBF).[14,15] Nevertheless, HA coating has been reported to exhibit poor bonding characteristics because of its notably different thermal expansion coefficient (CTE) with titanium alloys.[16] The CTE of some glass ceramics such as sphene ($CaTiSiO_5$),[17] monticellite ($CaMgSiO_4$),[18]

[1]Department of Medical Engineering, Qaemshar Islamic Azad University, Qaemshar, Iran
[2]Department of Materials Engineering, Babol Noshirvani University of Technology, Babol, Iran
[3]Cellular and Molecular Biology Research Center, Health Research Institute, Babol University of Medical Sciences, Babol, Iran
[4]Department of Mechanical Engineering, Politecnico di Milano, Milan, Italy

Corresponding author:
Sayed Mahmood Rabiee, Department of Materials Engineering, Babol Noshirvani University of Technology, Shariati Av, Babol 47148 - 71167, Iran.
Email: rabiee@nit.ac.ir

and akermanite ($Ca_2MgSi_2O_7$)[11] were recently reported to be closer to that of Ti6Al4V alloy. Akermanite, which is crystallized in a tetragonal lattice system and consists of magnesium oxide (MgO) tetrahedral and Si_2O_7 double-pyramid sheets linked together by CaO bonds,[19] is reported to exhibit not only adequate mechanical strength, but also high chemical stability and biocompatibility.[20] Ionic release of akermanite was shown to considerably enhance osteoblast cells' adhesion and proliferation.[11] These ions are key factors that influence the process of nucleation and growth of HA, and are reported to affect the mineralization process and the bone-bonding mechanism.[21] There are also indications that Ca and silicon (Si) released from bioactive glass dissolution can promote apatite formation, and stimulate osteoblast proliferation and gene expression.[22]

Considering the efficiency of ceramic coatings on biomedical implants, various methods including plasma spray, sol-gel, and electrophoretic deposition (EPD) have been suggested for their deposition.[17] Herein, we used the sol-gel method to coat Ti6Al4V substrates with a nanostructured akermanite ($Ca_2MgSi_2O_7$). The sol-gel method was used specifically for its advantages over other commonly used methods, including lower process temperature, providing the possibility of producing nanoscale particles and lower costs in addition to the flexibility of use for both coating and powder production.[23] Mg ions were incorporated into the synthesized coating, as it has been suggested that they can significantly enhance osteoblast adhesion and stimulate osteoblast proliferation.[24–26] Lack of Mg is also reported to contribute to reduced bone formation and cause osteoporosis.[27] Furthermore, Mg is known to facilitate more than 300 enzymic reactions in the human body.[28] Scanning electron microscopy (SEM), transmission electron microscopy (TEM), and atomic force microscopy (AFM) methods have been used to study the morphology and structure of the obtained coating. X-ray diffraction (XRD) and energy-dispersive X-ray spectrum (EDX) were applied to examine phase composition and elements on the coating, respectively. In vitro tests were also performed to evaluate adhered cell morphology and proliferation on the coated samples.

Materials and Methods

Substrate Preparation

Disc-shaped Ti6Al4V samples with a diameter of 2 cm and thickness of 0.1 cm were sequentially polished by silicon carbide papers ranging from 100 to 600 grit sizes. The samples were subsequently ultrasonically washed in acetone for 15 minutes.

Coating Preparation and Characterization

Akermanite powder was synthesized by the sol-gel method using $(C_2H_5O)_4Si$ (TEOS), $Mg(NO_3)_2.6H_2O$, and $Ca(NO_3)_2.4H_2O$ as precursors of Si, Mg, and Ca, respectively. Briefly, tetraethyl orthosilicate (TEOS) was mixed with water and nitric acid (2N HNO_3, as a precipitant) and stirred for 30 minutes. Afterward, $Mg(NO_3)_2.6H_2O$ and $Ca(NO_3)_2.4H_2O$ was added to the solutions with a molar ratio of $TEOS/Mg(NO_3)_2.6H_2O/Ca(NO_3)_2.4H_2O = 2:1:2$. The mixture was then stirred at room temperature for 5 hours. For microstructure observation, dry gel of the prepared akermanite was characterized by TEM (EM208S). The distribution of akermanite particles was analyzed by EDX-mapping analysis.

The Ti6Al4V discs were fixed on a sol-gel coating (dip-coating) machine and were placed into the akermanite solution for 10 seconds. Samples were entered vertically in the solution at an approximate speed of 0.5 m per second and then with the same speed out of the solution. After being heat-treated at 900°C for 2 hours, the samples were characterized by a Philips PW3710 XRD instrument. The particle size was estimated using the Scherrer equation described in Equation 1:[29]

$$t = 0.89\,\lambda / \beta \cos\theta$$

Where t, λ, and β stand for grain size, wavelength, and diffraction peak width at half maximum height (in radians), respectively, and θ is the Bragg angle.

A Philips XL30 SEM was used for coated surface observation as well as coating thickness evaluation. The surface morphologies of the coated and uncoated samples were studied using FlexAFM (Switzerland).

Cell Culture

Coated and uncoated samples were sterilized in an autoclave at 120°C for 30 minutes. Then, the samples were incubated in Dulbecco's modified Eagle's medium (DMEM) and supplemented with 10% fetal bovine serum before cell seeding. The DMEM concentration was prepared according to previously published research.[30] SaSo-2 osteoblast cells were seeded on the samples and the culture medium was changed every 2 days. The culture was kept at 37°C in a humidified atmosphere of 95% air and 5% CO_2. A total of 5×10^4 cells passaged at these experiments. The culture media was changed every 2 days during the proliferation assay. After 3 days, the adhered cells were fixed with 2.5% glutaraldehyde buffer for 30 minutes at 4ºC. A dehydration process was performed using a graded ethanol solution of 30%, 50%, 70%, 95%, and 100%. Adhered cells' morphology was observed by SEM (VEGA TESCAN) and optical microscopy (OM). 3-(4,5-dimethylthiazol-2-yl)-2,5-diphenyl-2H-tetrazolium bromide (MTT) assay was used to assess the cells' viability on coated, uncoated, and control samples after 1, 3, and 7 days in culture. Ultra-high–molecular weight polyethylene (culture plate) was

used as negative control. The discs were kept under the same culture conditions with 720 μL of fresh culture medium and 80 μL of MTT solution. Subsequently, dimethyl sulfoxide was added to completely dissolve the purple formazan. The cell viability percentage was estimated by spectrophotometry (enzyme-linked immunosorbent assay reader) at a wavelength of 570 nm. A P value $<.05$ was determined to be statistically significant.

Results and Discussion

The XRD pattern of the coating (Figure 1) confirms the presence of $Ca_2MgSi_2O_7$ peaks (according to Joint Committee on Powder Diffraction Standards 00-076-0841). Akermanite is known to crystallize at temperatures above 700°C and to develop the crystalline phase by heat treatment at 800°C.[31] On the other hand, the Ti6Al4V surface is seriously damaged above 900°C.[32] Therefore, a heat treatment was applied at 900°C with the aim of increasing the crystallinity, reducing the residual stresses, and enhancing ductility without creating tension between the coating and the underlying titanium substrate and not damaging the coating and the substrate.[33] Peaks observed in Figure 1 can be considered as an indication of the high crystallinity of the coating. Few impurities of merwinite ($Ca_3MgSi_2O_8$) are present in the XRD pattern. The rutile peaks detected by XRD are also due to the limited thickness of the coating layer. The akermanite grain size was measured to be about 32 $\pm$ 2.5 nm according to the Scherrer equation.

TEM observation of the synthesized powder (Figure 2A) demonstrated nanosize powder particles with an almost oval shape and a smooth surface morphology. Figure 2B shows an SEM a top-surface micrograph of the synthesized coating. The micrograph indicates that the obtained coating has a disordered surface morphology

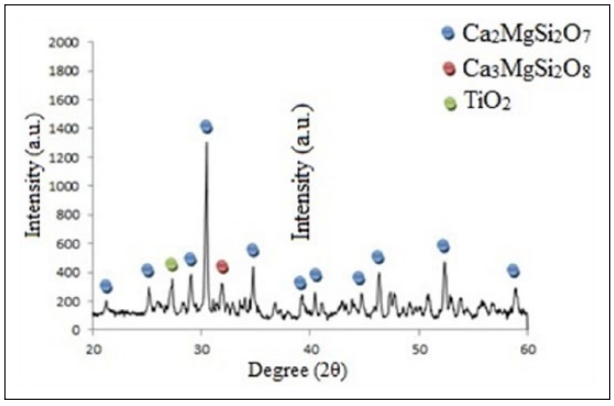

Figure 1. XRD Pattern of the Synthesized Coating at 900°C
$Ca_2MgSi_2O_7$ indicates akermanite glass-ceramic; TiO_2, titanium dioxide; XRD, X-ray diffraction.

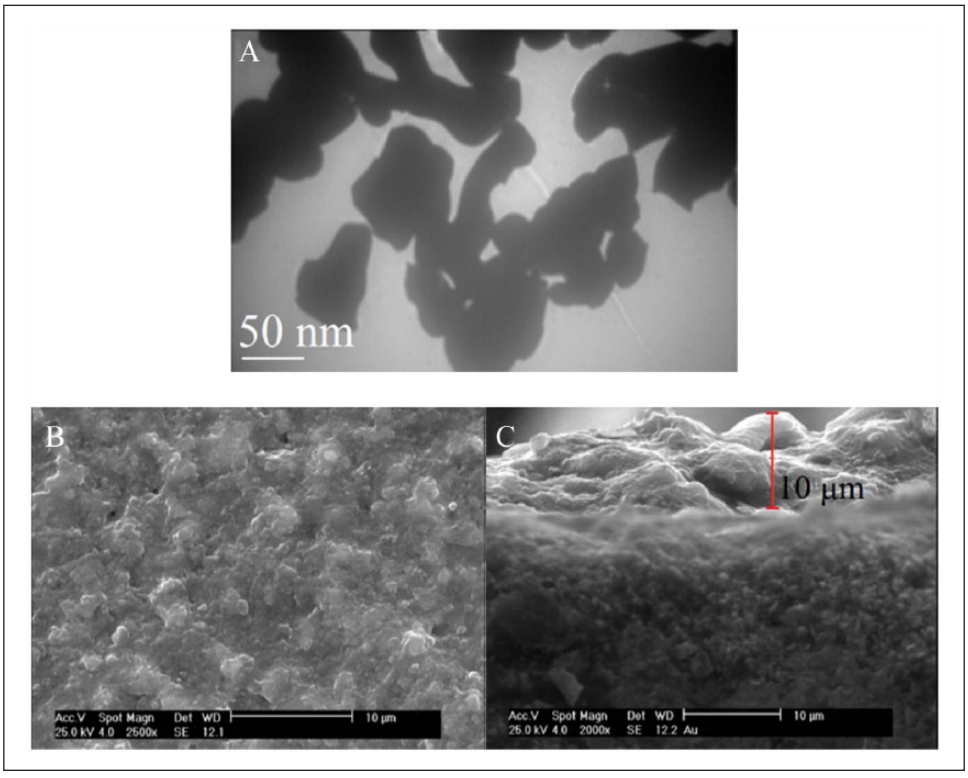

Figure 2. A, Transmission Electron Microscopy Micrograph of the Synthesized Powder; B, Scanning Electron Microscopy (SEM) Micrographs of the Coating Top Surface; and C, SEM Cross-Section Observation of the Coating.

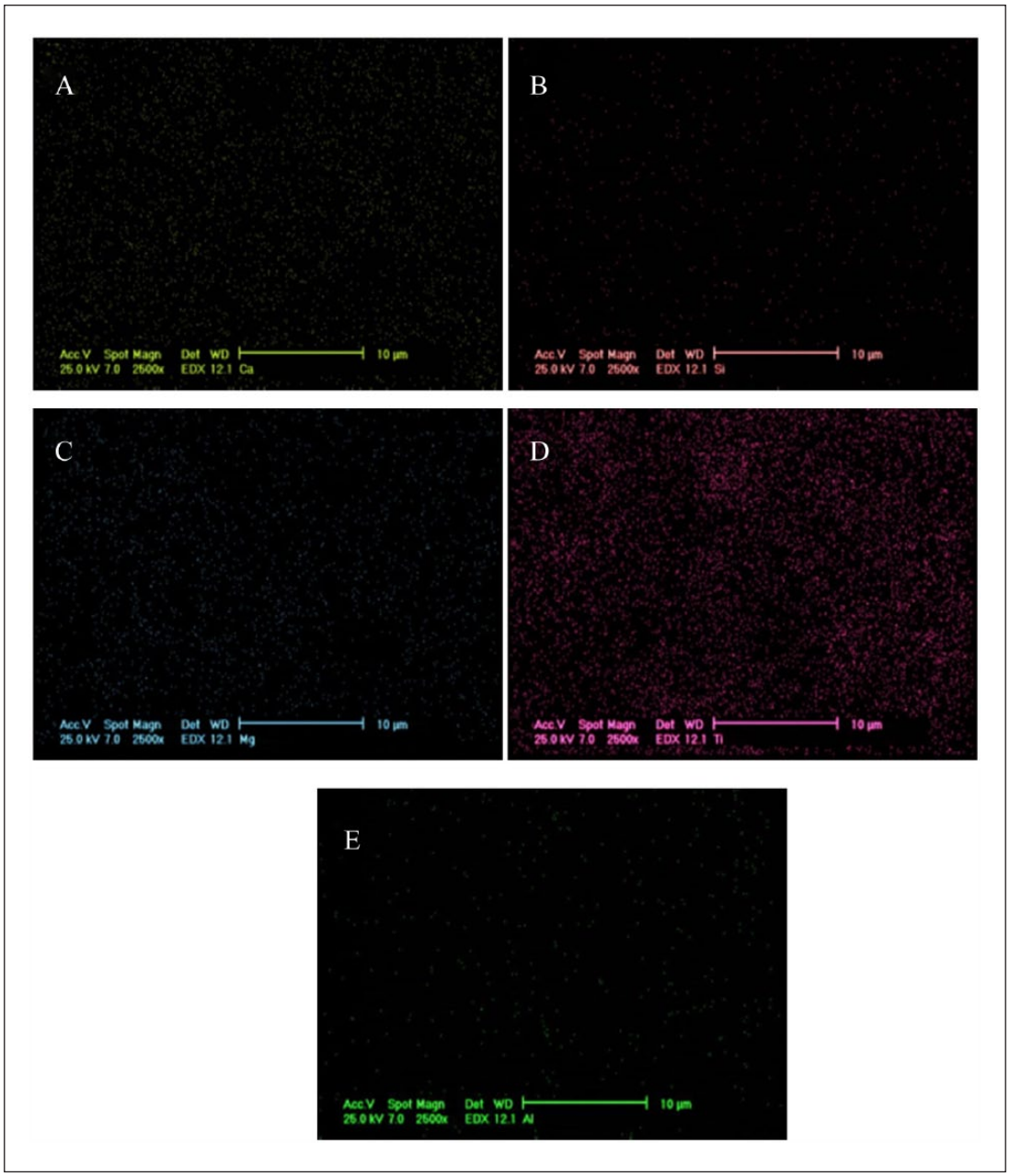

Figure 3. Energy-Dispersive X-Ray Spectrum (Mapping Results of Chemical Elements' Distribution, A, Calcium (Ca); B, Silicon (Si); C, MAGNESIUM (Mg); D, Titanium (Ti); and E, Aluminum (Al) on Surface Samples.

with the presence of some pores. The cross-section observation in Figure 2B displays a uniform and crack-free structure that is deposited uniformly all over the substrate. The coating thickness is quite regular and is measured to be about 5-10 μm with a defect-free microstructure. According to SEM observations, the created coating shows a disordered topography that is also confirmed by AFM analysis. EDX mapping analysis confirmed the presence of Ca, Si, Mg, Ti, and Al elements on the surface of the coated sample (Figure 3). The EDX cartography of the akermanite coating showed that all akermanite elements have been preserved in deposited nanostructures and are uniformly spread all over the sample's surface. The presence of the elements on the surface is expected to induce coating bioactivity, which can significantly promote the formation of HA.[27]

AFM images of the coated and uncoated surfaces, shown in Figure 4, exhibit a significantly higher surface roughness for the coated samples compared to the bare material (radium = 1.5 µm vs 0.1 µm). The coated surface

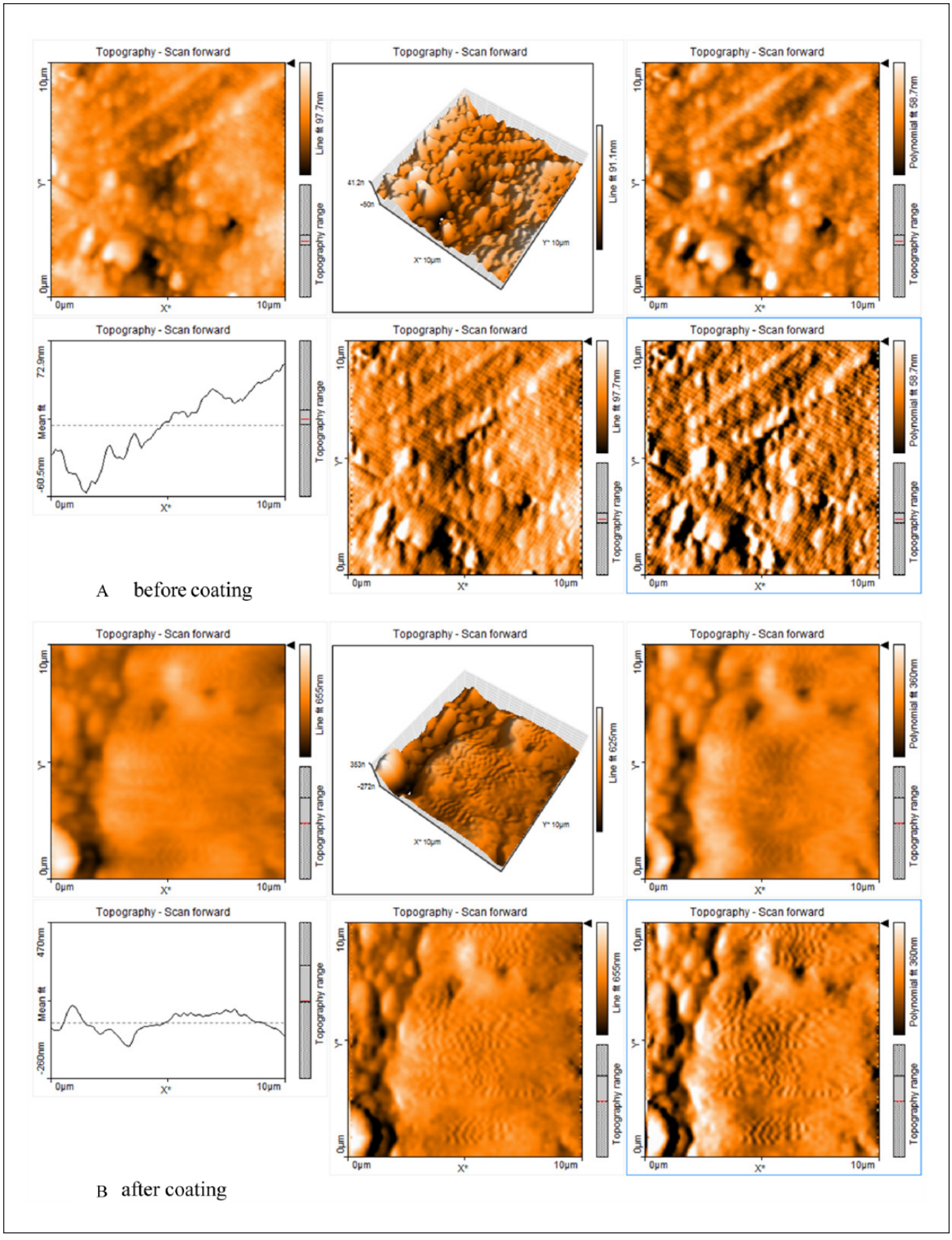

Figure 4. Atomic Force Microscopy Images A, Before Coating, and B, After Coating.

represents random surface topography. This hierarchical surface topography is expected to have positive effects on cellular activity.[34] The positive effects of micrometer-sized roughness of biomaterials on osteoblast behaviors have been well documented.[35] Disordered topography, as is the case for most biological tissue and almost all clinically

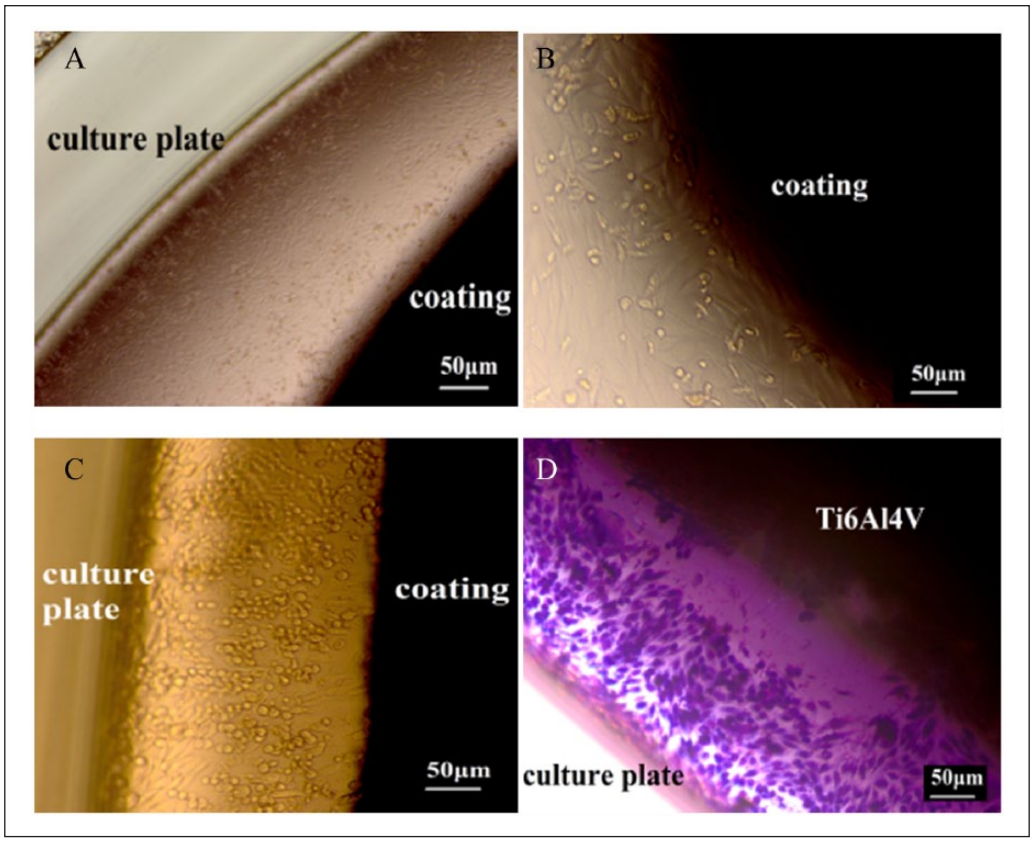

Figure 5. Optical Microscopy Images of Saos-2 Cells Cultured on A, B, Coated and C, D, Uncoated Discs After 3 Days. Magnification A, 40× and 200×, and D, 100× and C, 200×.

accepted biomaterials, is reported to highly affect the morphology of osteoblast cells.[36]

Figures 5 and 6 shows the OM and SEM micrographs representing the morphology of Saos-2 cells cultured on coated and uncoated samples after 3 days in culture. The cells cultured on the coated surface represent a rather flat morphology whereas the cultures on uncoated samples represent a more rounded configuration. SEM images under higher magnification confirm the higher tendency of the cells to spread in a more flattened configuration on the coated samples compared to the uncoated ones.

Calcified surface of the samples is shown in Figure 6. Calcification is the process by which mineral Ca builds up on biomaterials, and it is proved to have an important role in the bone bonding flow of bioglass and glass-ceramic bone implants.[24] This process depends on various factors including absorption of Ca-binding proteins on implant surface and cellular response of the host tissue to the biomaterials.[37,38] Also, the effect of Mg in this process is well documented.[38,39] The SEM images confirm good adhesion and anchorage of the cells to the surface coatings that can in turn confirm the cytocompatibility of the synthesized coatings.

Figure 7 shows the cell proliferation results of the MTT assay on coated and uncoated samples as well as control samples up to 1, 3, and 7 days in culture. The cultured Saos-2 osteoblast showed a significantly ($P < .05$) higher proliferation rate at 1, 3, and 7 days compared to the control sample. The results indicate that cell viability increased significantly on the coated samples in comparison with the uncoated ones at all time steps.

Conclusions

The sol-gel method was used to synthesize a nanocrystallized $Ca_2MgSi_2O_7$ coating on Ti6Al4V substrates. The obtained results indicate that akermanite phase can be synthesized from a gel precursor by calcining at 900°C. XRD, EDX, and microscopical analysis confirmed that the coating presented a defect-free and homogeneous nanostructure. In vitro assays with microscopical observation and cell-proliferation tests revealed that the obtained samples' coatings stimulated cell spreading compared to uncoated samples. The coating samples were found to effectively enhance cell-proliferation rate. The results reveal the adeptness of the synthesized coating in promoting cell interaction with bone implants, promising an improved tissue response.

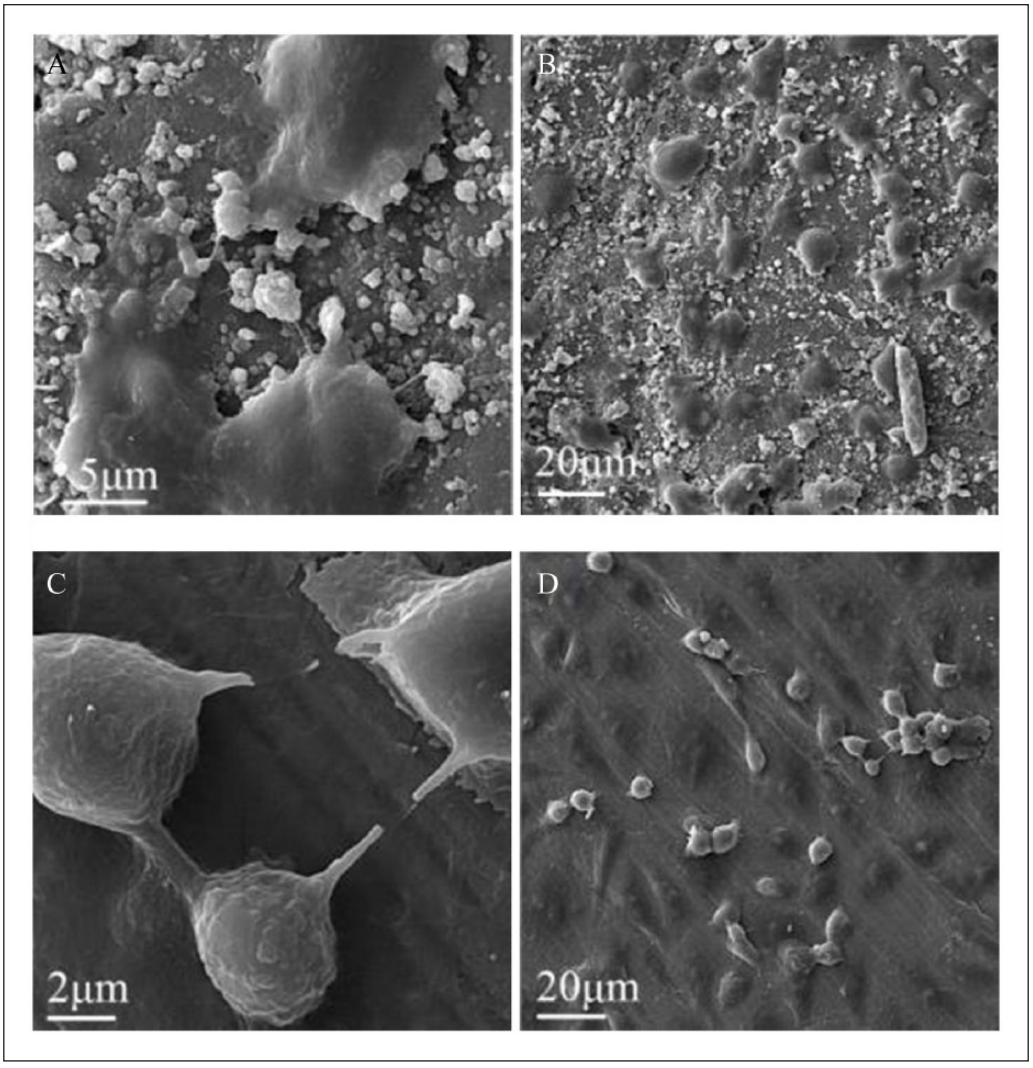

Figure 6. Scanning Electron Microscopy Images of Saos-2 Cells Cultured on Ti-6Al-4V A, B with Coating, and Ti-6Al-4V C, D, without Coating After 3 Days in Culture.

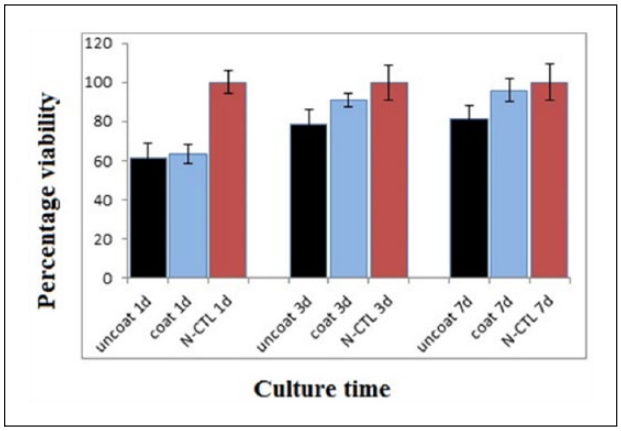

Figure 7. MTT Assay of the Samples After Different Culturing Times

d indicates days; MTT, 3-(4,5-dimethylthiazol-2-yl)-2,5-diphenyl-2H-tetrazolium bromide; N-CTL, negative control.

Declaration of Conflicting Interests

The author(s) declared no potential conflicts of interest with respect to the research, authorship, and/or publication of this article.

Funding

The author(s) received no financial support for the research, authorship, and/or publication of this article.

References

1. Niinomi M. Mechanical biocompatibilities of titanium alloys for biomedical applications. *J Mech Behav Biomed Mater* 2008; 1: 30–42.
2. Niinomi M. Recent research and development in titanium alloys for biomedical applications and healthcare goods. *Sci Technol Adv Mater* 2003;4(5):445–454.
3. Geetha M, Singh AK, Asokamani R, et al. Ti based biomaterials, the ultimate choice for orthopedic implants—a review. *Prog Mater Sci* 2009; 54: 397–425.

4. Ramaswamy Y, Wu C, Dunstan C, et al. Sphene ceramics for orthopedic coating applications: An in vitro and in vivo study. *Acta Biomater* 2009; 5: 3192–3204.
5. Yi D, Wu C, Ma B, et al. Bioactive bredigite coating with improved bonding strength, rapid apatite mineralization and excellent cytocompatibility. *J Biomater Appl* 2014; 28: 1343–1353.
6. Razavi M, Fathi M, Savabi O, et al. Controlling the degradation rate of bioactive magnesium implants by electrophoretic deposition of akermanite coating. *Ceram Int* 2014; 40: 3865–3872.
7. Mondragón-Cortez P and Vargas-Gutiérrez G. Electrophoretic deposition of hydroxyapatite submicron particles at high voltages. *Mater Lett* 2004; 58: 1336–1339.
8. Pang X, Casagrande T and Zhitomirsky I. Electrophoretic deposition of hydroxyapatite-$CaSiO_3$-chitosan composite coatings. *J Colloid Interface Sci* 2009; 330: 323–329.
9. Kim HW, Kim HE and Knowles JC. Improvement of hydroxyapatite sol–gel coating on titanium with ammonium hydroxide addition. *J Am Ceram Soc* 2005; 88: 154–159.
10. Xue W, Liu X, Zheng X, et al. In vivo evaluation of plasma-sprayed wollastonite coating. *Biomaterials* 2005; 26: 3455–3460.
11. Yi D, Wu C, Ma X, et al. Preparation and in vitro evaluation of plasma-sprayed bioactive akermanite coatings. *Biomed Mater* 2012; 7: 065004.
12. Maleki-Ghaleh H, Hafezi M, Hadipour M, et al. Effect of tricalcium magnesium silicate coating on the electrochemical and biological behavior of Ti-6Al-4V alloys. *PLoS One* 2015; 10: e0138454.
13. Pan YK, Chen CZ, Wang DG, et al. Influence of additives on microstructure and property of microarc oxidized Mg–Si–O coatings. *Ceram Int* 2012; 38: 5527–5533.
14. Xu S, Lin K, Wang Z, et al. Reconstruction of calvarial defect of rabbits using porous calcium silicate bioactive ceramics. *Biomaterials* 2008; 29: 2588–2596.
15. Xiaoni H, Guangfu Y, Xianchun C, et al. Effect of akermanite morphology on precipitation of bone-like apatite. *Appl Surf Sci* 2001; 257: 3417–3422.
16. Mohammadi H and Sepantafar M. Ion-doped silicate bioceramic coating of Ti-based implant. *Iran Biomed J* 2016; 20: 189–200.
17. Wu C, Ramaswamy Y, Gale D, et al. Novel sphene coatings on Ti-6Al-4V for orthopedic implants using sol-gel method. *Acta Biomater* 2008; 4: 569–576.
18. Chen X, Ou J, Kang Y, et al. Synthesis and characteristics of monticellite bioactive ceramic. *J Mater Sci Mater Med* 2008; 19: 1257–1263.
19. Ochi Y. Crystal structure of Sr-akermanite glass–ceramics. *Mater Res Bull* 2006; 4: 1825–1834.
20. Wu C, Chang J, Ni S, et al. In vitro bioactivity of akermanite ceramics. *J Biomed Mater Res A*. 2006; 76: 73–80.
21. Dufrane D, Delloye C, McKay I, et al. Indirect cytotoxicity evaluation of pseudowollastonite. *J Mater Sci Mater Med* 2003; 14: 33–38.
22. Gough JE, Jones JR and Hench LL. Nodule formation and mineralisation of human primary osteoblasts cultured on a porous bioactive glass scaffold. *Biomaterials* 2004; 25: 2039–2046.
23. Lutišanová G, Palou MT and Kozánková J. Comparison of bioactivity in vitro of glass and glass ceramic materials during soaking in SBF and DMEM medium. *Journal Ceramics-Silikáty* 2011; 55: 199–207.
24. Hickey DJ, Ercan B, Sun L, et al. Adding MgO nanoparticles to hydroxyapatite-PLLA nanocomposites for improved bone tissue engineering applications. *Acta Biomater* 2015; 14: 175–184.
25. Witte F, Kaese V, Haferkamp H, et al. In vivo corrosion of four magnesium alloys and the associated bone response. *Biomaterials* 2005; 26: 3557–3563.
26. Bagherifard S. Mediating bone regeneration by means of drug eluting implants: From passive to smart strategies. *Mater Sci Eng C Mater Biol Appl* 2017; 71: 1241–1252.
27. Smith B and Nisbet D. Biochemical and pathological studies on magnesium deficiency in the rat: II. Adult animals. *J Comp Pathol* 1972; 82: 37–46.
28. Tiwari A and Nordin AN (eds) *Advanced biomaterials and biodevices*. Hoboken, NJ: John Wiley & Sons, 2014.
29. Fu J. Long-lasting phosphorescence of transparent surface-crystallized glass-ceramics. *J Am Ceram Soc* 2004; 83: 2613–2615.
30. Allu AR, Tulyaganov DU, Mather GC, et al. Influence of strontium oxide on structural transformations in diopside-based glass-ceramics assessed by diverse structural tools. *J Phys Chem C* 2015; 119: 11482–11492.
31. Ventura JMG, Tulyaganov DU, Agathopoulos S, et al. Sintering and crystallization of akermanite-based glass-ceramics. *Mater Lett* 2006; 60: 1488–1491.
32. Wu C, Ramaswamy Y, Liu X, Wang G and Zreiqat H. Plasma-sprayed $CaTiSiO_5$ ceramic coating on Ti-6Al-4V with excellent bonding strength stability and cellular bioactivity. *J R Soc Interface* 2009; 6: 159–168.
33. Wu C, Chang J, Wang J, et al. Preparation and characteristics of a calcium magnesium silicate (bredigite) bioactive ceramic. *Biomaterials* 2005; 26: 2925–2931.
34. Bagherifard S, Hickey DJ, de Luca AC, et al. The influence of nanostructured features on bacterial adhesion and bone cell functions on severely shot peened 316L stainless steel. *Biomaterials* 2015; 73: 185–197.
35. Zhao G, Raines AL, Wieland M, et al. Requirement for both micron and submicron scale structure for synergistic responses of osteoblasts to substrate surface energy and topography. *Biomaterials* 2007; 28: 2821–2829.
36. Yang L, Gong Z, Lin Y, et al. Disordered topography mediates filopodial extension and morphology of cells on stiff materials. *Adv Funct Mater* 2017; 27: 1702689.
37. Khalili V, Khalil-Allafi J, Xia W, et al. Preparing hydroxyapatite-silicon composite suspensions with homogeneous distribution of multi-walled carbon nano-tubes for electrophoretic coating of NiTi bone implant and their effect on the surface morphology. *Appl Surf Sci* 2016; 366: 158–165.
38. Althoff J, Quint P, Krefting ER, et al. Morphological studies on the epiphyseal growth plate combined with biochemical and X-ray microprobe analyses. *Histochemistry* 1982; 74: 541–552.
39. Liu Q, Cen L, Yin S, et al. A comparative study of proliferation and osteogenic differentiation of adipose-derived stem cells on akermanite and beta-TCP ceramics. *Biomaterials* 2008; 29: 4792–4799.